Research Paper

PAIN

OPEN

Netrin-1 receptor DCC is required for the contralateral topography of lamina I anterolateral system neurons

Farin B. Bourojeni[a,b], Hanns Ulrich Zeilhofer[c,d], Artur Kania[a,b,e,*]

Abstract

Anterolateral system (AS) neurons relay nociceptive information from the spinal cord to the brain, protecting the body from harm by evoking a variety of behaviours and autonomic responses. The developmental programs that guide the connectivity of AS neurons remain poorly understood. Spinofugal axons cross the spinal midline in response to Netrin-1 signalling through its receptor deleted in colorectal carcinoma (DCC); however, the relevance of this canonical pathway to AS neuron development has only been demonstrated recently. Here, we disrupted Netrin-1:DCC signalling developmentally in AS neurons and assessed the consequences on the path finding of the different classes of spinofugal neurons. Many lamina I AS neurons normally innervate the lateral parabrachial nucleus and periaqueductal gray on the contralateral side. The loss of DCC in the developing spinal cord resulted in increased frequency of ipsilateral projection of spinoparabrachial and spinoperiaqueductal gray neurons. Given that contralateral spinofugal projections are largely associated with somatotopic representation of the body, changes in the laterality of AS spinofugal projections may contribute to reduced precision in pain localization observed in mice and humans carrying *Dcc* mutations.

Keywords: nociception, anterolateral, spinofugal, spinoparabrachial, spinothalamic, commissural, Hoxb8, DCC, Netrin-1, lamina I, projection neurons

1. Introduction

Nociception involves spinal neural circuit processing of noxious stimuli and their relay to nociceptive brain centres such as the thalamus, the lateral parabrachial nucleus (LPbN), and the periaqueductal gray (PAG).[1] This is accomplished by anterolateral system (AS) spinofugal neurons, whose axons ascend in the anterolateral tract of the spinal cord. The ventral posterolateral (VPL) thalamus relays somatotopically organized nociceptive inputs to the somatosensory cortex,[5] a pathway associated with the sensory-discriminative aspects of pain. The LPbN has been associated with the affective-emotional components of nociception,[36] whereas the PAG is involved in escape/defense responses.[27,67] Despite extensive anatomical studies of AS neurons, how their connectivity is specified is largely unknown.

Anterolateral system neuronal function has been inferred from their anatomy and physiology. In rodents, these are primarily confined to lamina I of the superficial dorsal horn (SDH), the deep dorsal horn (DDH; lateral lamina V), and the lateral spinal nucleus (LSN).[46] Lamina I AS neurons in the SDH have small receptive fields[80] and respond to discrete nociceptive stimuli that, for example, induce thermal or mechanical pain sensation.[2,16,25] By contrast, lamina V/LSN AS neurons have broad receptive fields and wide dynamic range receptivity, such as activation by a variety of noxious and innocuous stimuli.[17] Because of their extensive projections to the dorsal LPbN[29] and the medial thalamus,[33] lamina V/LSN AS neurons are likely to transmit the affective-motivational aspects of nociception. Most lamina I AS neurons innervate their brain targets on the contralateral side,[72] whereas the proportions of lamina V/LSN AS neurons that project ipsilaterally and contralaterally are more similar.[19,46] One possibility is that the laterality of lamina I AS neurons is an essential part of their somatotopic organization, allowing localization or topognosis, of noxious stimuli.

During development, axons of spinal projection neuron either cross the midline at the floor plate or remain on the ipsilateral side, and then grow rostrally to their target, in specific white matter tracts.[34] The molecular mechanisms that control midline crossing are mostly elucidated,[11] although their perturbation has provided few insights into adult neural circuit function. Netrin-1 signalling through its receptor deleted in colorectal carcinoma (DCC) is a principal determinant of commissural crossing.[23,45,52,78,82] Developmental perturbations of Netrin-1:DCC signalling result in abnormal motor behaviour in mice and humans, presumably caused by decreased midline crossing by spinal interneurons and

Sponsorships or competing interests that may be relevant to content are disclosed at the end of this article.

[a] Research Unit in Neural Circuit Development, Institut de Recherches Cliniques de Montréal (IRCM), Montréal, QC, Canada, [b] Integrated Program in Neuroscience, McGill University, Montréal, QC, Canada, [c] Institute of Pharmacology and Toxicology, University of Zurich, Zurich, Switzerland, [d] Institute of Pharmaceutical Sciences, Swiss Federal Institute of Technology (ETH) Zurich, Switzerland, [e] Division of Experimental Medicine, Department of Anatomy and Cell Biology, McGill University, Montréal, QC, Canada

**Corresponding author. Address: Institut de recherches cliniques de Montréal (IRCM)110, avenue des Pins Ouest Montréal (Québec), Canada H2W 1R7. E-mail address: artur.kania@ircm.qc.ca (A. Kania).*

PAIN 162 (2021) 161–175

http://dx.doi.org/10.1097/j.pain.0000000000002012

corticospinal axons.[63,64,73] However, the role of Netrin-1:DCC signalling in AS neuron development and function is only beginning to emerge. Loss of embryonic DCC expression in the caudal spinal cord (*Dcc* spinal knockout; Dcc^{SpKO}) results in increased ipsilateral innervation of the thalamus by spinothalamic (ST) neurons and inability to accurately localize noxious stimuli. Humans with mirror movement disorder caused by *DCC* mutations also display a similar phenotype. Despite this, the impact of spinal *Dcc* mutation on the laterality of most AS spinofugal pathways remains unknown, hindering accurate interpretations of their specific roles in nociception. Here, we describe the temporal and spatial aspects of *Hoxb8::Cre* expression and present evidence of AS neuron connectivity changes as a result of Dcc^{SpKO} mutation (*Hoxb8::Cre;* $Dcc^{flox/-}$).

2. Materials and methods

2.1. Mouse lines and animal care

All mice were housed at the Animal Housing core facility of Institut de recherches cliniques de Montréal, kept on a 12:12-hour light/dark cycle, and provided food and water ad libitum. All experimental procedures were approved by the Animal Care and Use Committee at the Institut de recherches cliniques de Montréal, in accordance with the regulations of the Canadian Council on Animal Care. The generation of *Hoxb8::Cre* mice has been described previously.[81] Cre-dependent reporter lines *R26:LS-tdTomato*[50] and *Tau:LS-mGFP-nLacz*[38] were obtained from the Jackson Laboratory (#007914 and #021162). $Dcc^{flox/-}$ were generated from crossing of $Dcc^{flox/flox}$[48] and $Dcc^{+/-}$,[28] both obtained from F. Charron (**Table 1** for details).

2.2. Tissue harvest and immunohistochemistry

Animals were anaesthetized with an intraperitoneal injection of ketamine/xylazine solution (10 mg/mL ketamine, 1 mg/mL xylazine, in 0.9% saline; dose: 0.1 mL/g body weight). They were then transcardially perfused with 15 mL of a 0.9% saline solution followed by an equal volume of 4% paraformaldehyde (PFA) in 1 M phosphate buffered saline (PBS). Brain and spinal cord tissues were harvested and postfixed with PFA for 1 hour at 4°C while shaking. Embryos were dissected in 4°C PBS and then transferred to 4% PFA for 1 to 2 hours at 4°C while shaking. The tissue was then cryoprotected in a 30% sucrose/PBS solution. Frozen spinal and DRG samples were sectioned at 25 μm and brain sections at 50 μm, collected on slides and kept frozen until use.[62] Alternatively, frozen embryonic samples were cut on a cryostat into 16-μm thick sections.

For immunostaining, the slides were rinsed 3 times with PBS and blocked with 5% horse serum prepared in PBS containing 0.1% Triton X-100. Upon 3 further rinses, the sections were treated with the appropriate primary antibodies (**Table 1** for details) overnight at 4°C. After PBS rinses, the samples were treated with fluorophore-conjugated secondary antibodies and counterstained with DAPI (4′,6-diamidino-2-phenylindole) for 2 hours at room temperature before coverslipping and imaging.

2.3. Retrograde tracing

Animals were first anaesthetized using 5% isoflurane/oxygen and maintained in 2% isoflurane/oxygen during the surgery. The head was immobilized in a stereotaxic frame (Kopf Instruments). The skin was incised to expose the underlying skull. A pulled glass needle backfilled with mineral oil was mounted in a syringe (Hamilton Company, Reno, NV) and then placed in a stereotaxic syringe pump with Micro4 controller (David Kopf Instruments, Tujunga, CA). Retrograde tracer cholera toxin B (CTB) conjugated to Alexa Fluor 488 was then loaded in the electrode from the tip. The glass capillary electrode tip was placed at the appropriate coordinates (LPbN: AP −5.35/ML 1.4/DV −3.05; PAG AP −4.5/ML 0.95/DV −2.55) from bregma (defined by the coronal Allen Brain Reference Atlas[24]), and a handheld drill was used to create a burr hole for the injection. A volume of 250 nL of tracer was injected at a rate of 100 nL/min in each target and the glass electrode was left in place for 2.5 minutes before removal to minimize tracer leakage. The skin was then sutured, and the mouse placed in a heated recovery chamber and allowed back into its cage once fully mobile. Spinal and brain tissues were harvested for analysis 7 days after the injection.

2.4. Intraspinal virus injections

A dorsal dermal incision of approximately 1.5 cm was made to expose the underlying vertebral column at the lumbar region.[47] To access the L3 to L5 spinal region, the connective and muscle tissues overlaying the intervertebral space between T13 and L1 vertebral segments were removed. The vertebral column was then immobilized in the stereotaxic frame to minimize respiration-induced mobility of the spinal column. A pulled glass needle backfilled with mineral oil was mounted in a syringe and then placed in a stereotaxic syringe pump with Micro4 controller (Kopf Instruments). The virus was then forward-pulled in the electrode. Three unilateral injections of 250 nL were made (ML 0.45 mm; AP 0 ± 0.5 mm; DV 0.35 mm dorsal spinal midline). The injections were each completed at a rate of 100 nL/minute followed by equal time for resting the needle to minimize leakage. Surrounding muscles were then sutured over the injection site and the skin stapled. The mouse was then placed in a heated recovery chamber and allowed back into its cage once fully mobile. Spinal and brain tissues were harvested for analysis 4 weeks after the injection.

2.5. Microscopy and image processing

Images were acquired with a confocal laser scanning microscope (Leica Microsystems, Inc., Wetzlar, Germany; TCS SP8) equipped with Leica Application Suite X. For cell count analysis, images captured using the inverted epifluorescent microscope (Leica Microsystems, Inc; Leica DM6) were deemed appropriate for quantification based on high signal/noise ratio. Image files were processed and analyzed in ImageJ (NIH). All presented figures and illustrations were assembled in Graphic (Picta, Inc).

2.6. Statistics

Quantification and statistical analyses were completed using Prism 8 (GraphPad, Inc). Nonparametric 2-tailed Mann–Whitney test was used for the quantifications in the 2 last figures.

3. Results

3.1. Hoxb8::Cre labels commissural neurons that express DCC during development

Hoxb8::Cre-driven excision of *Dcc* results in impaired nociceptive topognosis.[18] To uncover the extent to which AS neuron connectivity contributes to this phenotype, we first assessed the expression of *Hoxb8::Cre*. The AS consists of neurons that

Table 1

Resource table.

Reagents	Resource	Identifier (RRID)
Mice (MGI notation)		
Dcc$^{+/-}$ (*Dcc*^{tm1Wbg})	Frédéric Charron	MGI:3665466
Dcc$^{flox/flox}$ (*Dcc*$^{tm1.1Nki}$/*Dcc*$^{tm1.1Nki}$)	Frédéric Charron	MGI:5308804
Hoxb8::Cre (*Tg(Hoxb8-cre)1403Uze*)	Hanns Ulrich Zeilhofer	MGI:4881836
R26:LS-tdTomato (B6.Cg-*Gt(ROSA)26Sor*$^{tm14(CAG-tdTomato)Hze}$/J)	JAX	IMSR_JAX:007914
Tau:LS-mGFP-nLacz (B6;129P2-*Mapt*^{tm2Arbr}/J)	JAX	IMSR_JAX:021162
Antibodies (dilution)		
Chicken anti-β-galactosidase (1:2000)	Abcam	AB_307210
Goat anti-DCC (1:500)	R&D Systems	AB_2089765
Guinea pig anti-vGluT2 (1:1000)	Synaptic Systems	AB_887884
Mouse anti-Lhx2 (1:500)	DSHB	AB_2618817
Mouse anti-Lmx1b (1:10,000)	Thomas Müller & Carmen Birchmeier	AB_2314752
Mouse anti-NeuN (1:500)	Abcam	AB_2298772
Mouse anti-Nkx2.2 (1:500)	DSHB	AB_531794
Rabbit anti-DsRed (1:1000)	Clonetech	AB_10013483
Rabbit anti-GFP (1:1000)	Life Technologies	AB_221569
Rabbit anti-Iba1 (1:1000)	Wako	AB_839504
Rabbit anti-Sox2 (1:1000)	Abcam	AB_2341193
Rat anti-RFP (1:1000)	ChomoTek	AB_2336064
Donkey anti-chicken Cy5 (1:500)	Jackson ImmunoResearch	AB_2340365
Donkey anti-goat AF488 (1:500)	Jackson ImmunoResearch	AB_2336933
Donkey anti-guinea Pig AF488 (1:500)	Jackson ImmunoResearch	AB_2340472
Donkey anti-mouse AF488 (1:500)	Jackson ImmunoResearch	AB_2340846
Donkey anti-mouse Cy5 (1:500)	Jackson ImmunoResearch	AB_2340819
Donkey anti-rabbit AF488 (1:500)	Jackson ImmunoResearch	AB_2313584
Donkey anti-rabbit Cy3 (1:500)	Jackson ImmunoResearch	AB_2307443
Donkey anti-rat Cy3 (1:500)	Jackson ImmunoResearch	AB_2340683
Chemicals (dilution/concentration)		
DAPI (4′,6-diamidino-2-phenylindole) (1:500)	Life Technologies	AB_2629482
Neurotrace 450 (1:500)	Life Technologies	N/A; Cat# N21479
AlexaFluor488 cholera toxin B (1% weight/volume)	Life Technologies	N/A; Cat# C22841
Viruses (titre)		
AAV2.8-hSyn-SYP1-miniSOG-citrine (2.2E13 GC/mL)	Neurophotonics Centre, Université Laval	Addgene #50971

AAV, adeno-associated virus.

extend axons rostrally and innervate supraspinal targets in the brainstem and thalamus before birth.[19,75] To assess the expression of *Hoxb8::Cre* in spinal neurons, we first examined the temporal and spatial domains of Cre recombination by determining the onset of recombination in the developing caudal neural tube. *Hoxb8::Cre* mice were crossed to homozygous *R26:LS-tdTomato (Ai14)* reporter mice to generate *Hoxb8::Cre*$^{+/-}$; *R26:LS-tdTomato*$^{+/-}$ (*Hoxb8-tdTomato*) embryos that express the fluorescent protein tdTomato in Cre-expressing tissues. In 9.5-day-old embryos (E9.5), at a time when first spinal postmitotic neurons are generated in the cervical spinal cord,[60,79] tdTomato expression occurred predominantly in the caudal neural tube at spinal levels caudal to forelimbs (**Fig. 1A**). In sections of hind limb-level spinal cord, tdTomato expression was present throughout the mediolateral extent and dorsoventral extent of the neural tube without any apparent bias (**Figs. 1B and C**). At this stage, postmitotic neurons are yet to be generated in the caudal neural tube and all cells therein are neural progenitors expressing the stem cell marker Sox2. Sox2+ cells colocalized with tdTomato demonstrate that *Hoxb8::Cre*-driven recombination readily occurs in spinal neuron progenitors.

At E11.5, after the generation of postmitotic neurons, tdTomato expression was also observed throughout the dorsoventral extent of the spinal cord (**Figs. 1D and E**). The majority of commissural axons, thought to contribute to the AS, cross the spinal midline between E10 and E12, soon after the birth of commissural neurons.[11] We therefore asked whether *Hoxb8-tdTomato* expression overlaps with DCC, required for commissure crossing of many axons, including those of spinothalamic (ST) neurons (**Fig. 1E**). Virtually, all DCC-expressing E11.5 neurons throughout the dorsoventral extent of the neural tube coexpressed tdTomato (DsRed+; **Fig. 1F**; 5 sections/animal). Spinal commissural neurons arise from multiple postmitotic cardinal groups.[49,70] In particular, the dI1,[37] dI5,[74] and V3[83] clusters give rise to populations of commissural neurons, many of which project supraspinally (**Fig. 1G**). We observed expression of tdTomato within all 3 populations, identified through their respective transcription factor markers Lhx2, Lmx1b, and Nkx2.2 (**Figs. 1H–J**). Collectively, our results show that *Hoxb8::Cre* is expressed in classes of transcriptionally distinct commissural neurons that express DCC during development.

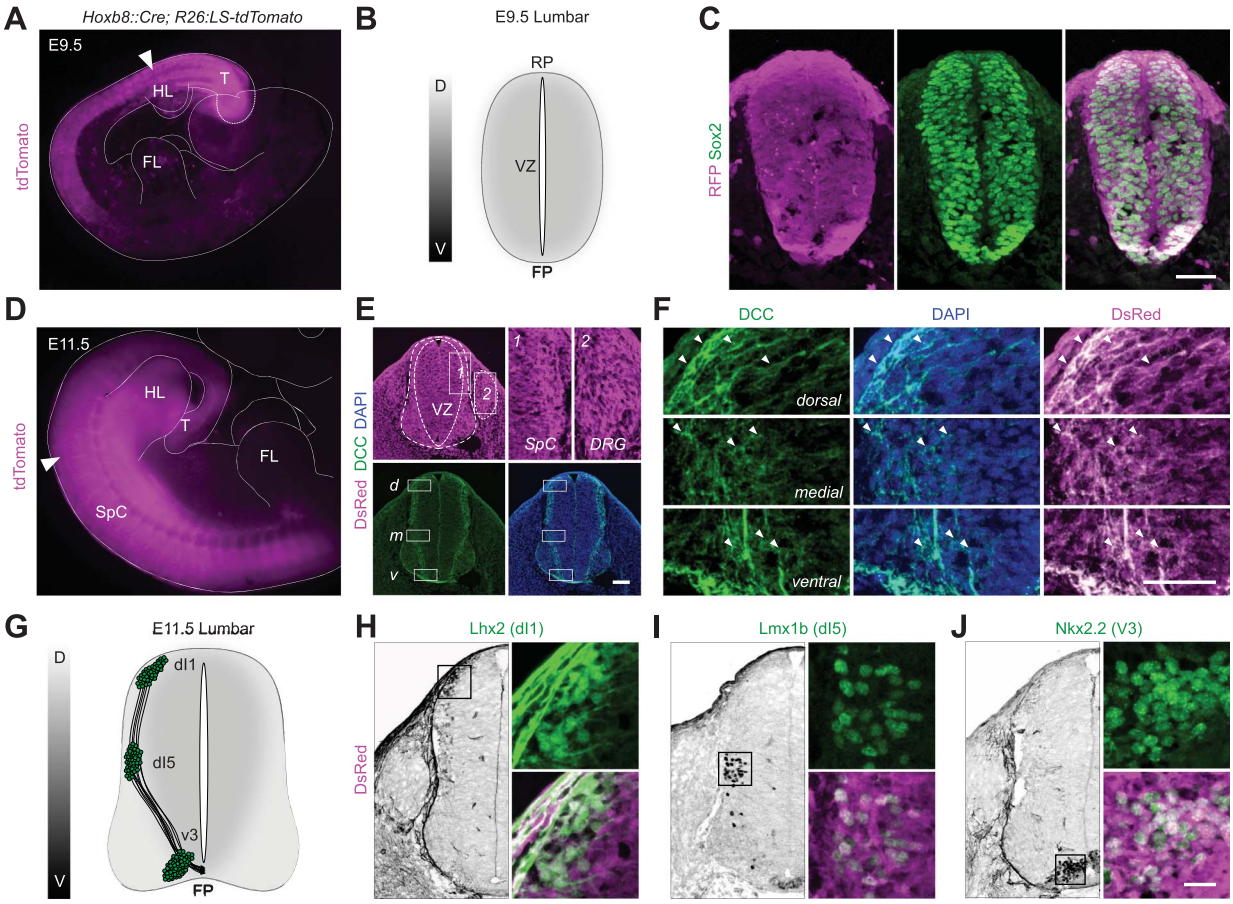

Figure 1. *Hoxb8::Cre* expression during the development of spinal commissural neurons. Fluorescent images of *Hoxb8-tdTomato* expression (magenta) in whole-mount embryos at embryonic day 9.5 (A) and 11.5 (D). White arrowheads in A and D designate the relative position of the cross-sections in C and E, respectively. (B) The neural tube at E9.5 largely comprises neural progenitors in the VZ. (C) Cre-driven reporter expression (RFP; magenta) highly colocalizes with progenitor cells marked by Sox2 expression (green) (n = 7; 3 sections/animal). (E) (Top row) Cross-sections of E11.5 caudal neural tube show extensive tdTomato expression in the postmitotic cells in the (1) spinal marginal zone (1) and (2) DRG cells. (Bottom row) Numerous commissural neurons express DCC in dorsal, medial, and ventral regions of the neural tube (in boxes and magnified in F) (F) tdTomato expression (RFP+) is detectable in dorsal, intermediate, and ventral spinal cord cells (arrowheads) that also express DCC (green) on their membranes (n = 4; 3 sections/animal). (G) Major populations of commissural neurons arise from the postmitotic cardinal groups dI1, dI5, and V3. (H–J) Extensive intersection of DsRed immunoreactivity (magenta) is detectable with transcriptional markers (green) of dI1 (Lhx2+), dI5 (Lmx1b+), and V3 (Nkx2.2+) (n = 4; 3 sections/animal). Scale bar: (C and F) 50 μm (E) 100 μm (H–J) 25 μm. D, dorsal; DRG, dorsal root ganglion; dI1, dorsal interneuron class 1; dI5, dorsal interneuron class 5; FL, forelimb; FP, floorplate; HL, hind limb; RP, roofplate; SpC, spinal cord; T, tail; V, ventral; VZ, ventricular zone; V3, ventral interneuron class 3.

3.2. Somatic Hoxb8::Cre expression is essentially absent from the brain

To determine the extent to which brain or peripheral sensory neuron *Hoxb8::Cre* expression may contribute to the phenotypes previously characterized in *Dcc*^{SpKO} mice,[61,62] we examined neuronal expression of *Hoxb8::Cre* outside of the spinal cord in adult tissue. In line with expression in caudal DRG at E12.5, *Hoxb8-tdTomato* expression was detected in all neurons in adult DRG caudal to the third cervical DRG (**Fig. 2A**). In addition to the spinal cord and DRG, sparse expression of neuronal tdTomato (NeuN+/DsRed+) was detectable in the anteroventral nucleus of the thalamus (**Figs. 2B and C**). We also observed numerous cells in the forebrain (in particular the cortex) and to a lesser extent in brainstem regions. These cells were commonly in close proximity to one another and interspersed in clusters of 20 to 30 units (**Fig. 2D**), and displayed a radial morphology characteristic of microglia. In agreement with a previous report of *Hoxb8*-driven cortical microglia expression,[10] virtually all the tdTomato-expressing cells in *Hoxb8-tdTomato* cortical sections were not labelled by the neuronal marker NeuN but expressed the microglial marker Iba1 (**Fig. 2D**). In addition, we observed occasional single tdTomato+ pyramidal neurons in the cortex and hippocampus (data not shown). These results complement the previous observations that *Hoxb8::Cre* recombination is highly present in DRG neurons but essentially absent from neurons located rostral to the spinal cord.[81]

To quantify the proportion of spinal neurons expressing the *Hoxb8::Cre* transgene, we generated *Hoxb8::Cre*$^{+/-}$*; Tau:LS-mGFP-nuclearLacZ*$^{+/-}$ (*Hoxb8-nLacZ*) adult mice. The expression of nuclear LacZ allowed us to label individual spinal neuron cell bodies, without confounding axonal labelling, allowing their quantification. This is particularly important in the dorsal horn of the spinal cord where most AS neurons are located. In whole-mounted adult *Hoxb8-nLacZ* spinal tissue, mGFP expression was visible throughout the cord at all levels caudal to midcervical segments (**Fig. 3A**). To visualize the location of neuronal cell bodies expressing *Hoxb8::Cre*, cross-sections from all levels of *Hoxb8-nLacZ* spinal cord tissue were stained with X-gal. Consistent with mGFP expression, LacZ+ nuclei were visible throughout the gray matter and white matter (**Fig. 3B**). In the cervical enlargement, nuclear LacZ expression attenuates approximately at the C4 level with most LacZ+ cells sparsely distributed in the dorsal horn (data

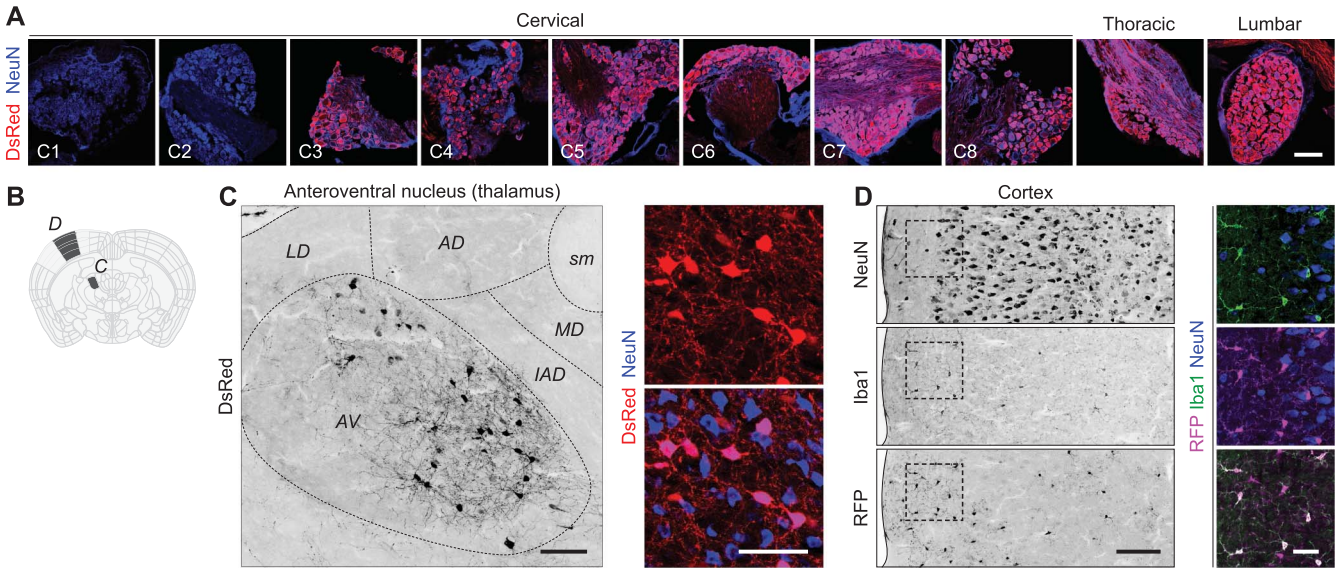

Figure 2. *Hoxb8::Cre* expression is detectable in selective nonspinal nuclei. (A) Nearly all DRG neurons (NeuN+; blue) caudal to cervical segment 3 (C3) including thoracic and lumbar express tdTomato (DsRed+; red) (n = 5; 3 sections/animal). (B) Schematic of the relative position of detected supraspinal tdTomato expression illustrated in C and D (bregma −0.88). In the brain, sparse neuronal expression of tdTomato (DsRed+/NeuN+) is detectable in (C) anteroventral nucleus of the thalamus. (D) In the cortex, RFP immunoreactivity (tdTomato+; magenta) is detectable in microglia (Iba1+; green) but not in neurons (NeuN; blue) (n = 7, 3 sections/animal). Scale bar: (A) 50 μm; (C) 100 μm, (inset) 25 μm; (C) 100 μm, (inset) 25 μm. AD, anterodorsal nucleus; AV, anteroventral nucleus; IAD, interanterodorsal nucleus; LD, lateral dorsal nucleus; MD, mediodorsal nucleus, sm, stria medullaris.

not shown). In the cervical segments C1 to C3, virtually no LacZ+ cells were detected. At midlumbar levels L3 to L5, the majority of spinal neurons (NeuN+) coexpressed β-galactosidase (**Fig. 3C**; 88.9% ± 1.35), indicating that *Hoxb8::Cre* is expressed in the majority of caudal spinal neurons.

We next examined *Hoxb8-tdTomato* expression in adult spinal tissue where tdTomato efficiently labels the cellular membrane, including the most distal extent of axons to supraspinal targets. In agreement with mGFP labelling in *Hoxb8-nLacZ* mice, tdTomato expression was detectable throughout the *Hoxb8-tdTomato* adult caudal spinal cord in both the white matter and gray matter (**Fig. 3D**). Using reporters driven by the ubiquitous *Rosa26* promoter or Tau (*MAPT*), we detected numerous cells with somatic expression of the reporter throughout the white matter suggesting that *Hoxb8::Cre* is expressed in both neuronal and nonneuronal progenitors (eg, glia or astrocytes). This expression is in agreement with reports that Tau is detectable in both neurons and to a lesser extent in glial cells.[43]

In the upper cervical segments, we identified axons primarily innervating the ventral horn (**Fig. 3D** right panel), in agreement with previous reports of intraspinal axonal projections from caudal propriospinal and motor circuits to upper cervical neurons.[26] We also detected dense axonal tdTomato expression in regions of the spinal white matter containing ascending projections (**Figs. 3D and E**). In particular, tdTomato-expressing axons were detectable in the dorsal and lateral white matter that encompass ascending sensory and motor pathways. Thus, the absence of neuronal expression of *Hoxb8-tdTomato* above cervical spinal levels implies that the fluorescent axons in the ascending white tracts at the cervical level originate from spinofugal neurons located more caudally.

3.3. Major motor and sensory spinofugal tracts are defined by Hoxb8::Cre expression

Given that supraspinal areas of the nervous system are spared from *Hoxb8::Cre* recombination, we reasoned that tdTomato+ axon terminals in the brain of *Hoxb8-tdTomato* mice must originate from spinofugal neurons. Most of these projections act as conduits of excitatory sensory inputs from the spinal cord to various brain regions involved in processing of sensory and motor information. To assess the innervation of supraspinal targets from the *Hoxb8::Cre*-expressing spinal domain, the brains from *Hoxb8-tdTomato* mice were transversely sectioned and immunostained for the neuronal marker NeuN and the glutamatergic presynaptic protein vGluT2 (vesicular Glutamate Transporter 2), to discriminate between passing and innervating axons. To enhance the detection of tdTomato, we used the anti-red fluorescent protein antibody (anti-DsRed). In *Hoxb8-tdTomato* mice, DsRed+ axon terminals were detected throughout the brain, although more frequently in the hind brain (**Fig. 4A**). We also detected substantial innervation of both sensory- and motor-related brain targets. In particular, in the hind brain, the DsRed+/vGluT2+ appositions were present in the dorsal column nucleus (**Fig. 4B** left), nucleus of the solitary tract (**Fig. 4B** right), intermediate and lateral reticular nuclei (**Fig. 4C** left), and inferior olivary complex (**Fig. 4C** right). The densely labelled tdTomato axon termini in the dorsal column nucleus represent the accumulation of both spinal[68] and primary afferents[57] that carry signals related to innocuous touch. Spinocerebellar axon terminals were visible in the granular layer of the central lobule of the cerebellum and were organized in columns (**Figs. 4D and E**). In the midbrain, the LPbN (**Fig. 4F**) and the PAG that are the principal targets of AS neurons had dense *Hoxb8-tdTomato* terminals (**Fig. 4G**). In addition, the motor-related pontine gray nucleus received many spinal inputs (**Fig. 4H**). Other sparsely innervated areas in the midbrain included the inferior colliculus and superior colliculus (data not shown). In the forebrain, all major somatosensory-related nuclei of the thalamus were also heavily innervated (**Fig. 4I**), including medial thalamic nuclei (**Fig. 4J**). Not surprisingly, the lateral spinothalamic pathway that primarily innervates the VPL (**Fig. 4K**) was well defined by *Hoxb8-tdTomato* axonal expression. Although evidence for a monosynaptic spinohypothalamic tract has been described in rats and cats,[9,44] no innervation of the medial hypothalamus by *Hoxb8-tdTomato* spinofugal neurons was detectable (data not shown). Instead, we only observed innervating

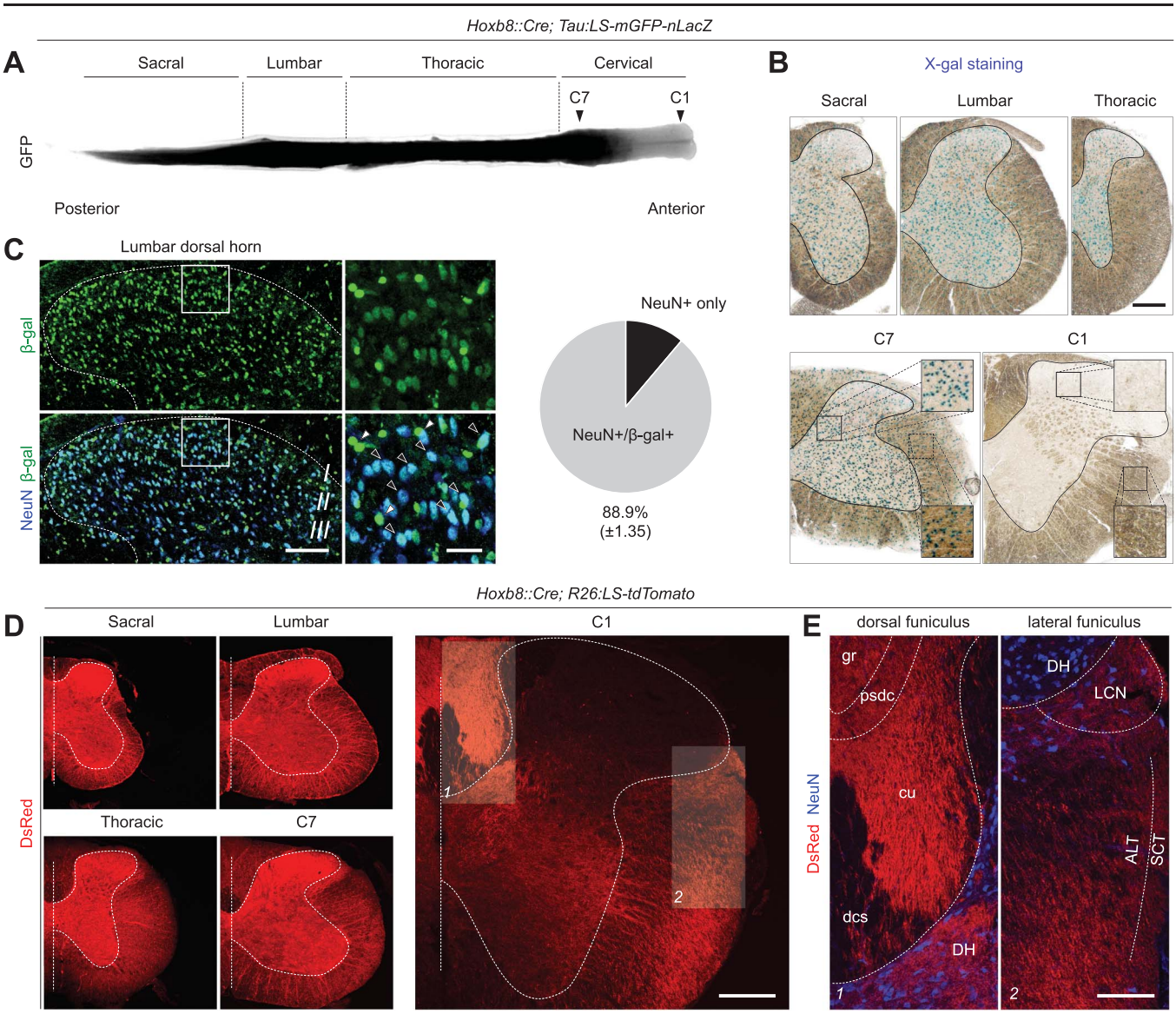

Figure 3. Characterization of *Hoxb8::Cre* expression in the spinal cord. (A) Dorsal view of whole-mount spinal cord of an adult *Hoxb8-nLacZ-mGFP* spinal cord showing inverted GFP fluorescence (black) caudal to midcervical segments. (B) Cross-sections of X-gal-stained segments throughout the spinal cord showing widespread β-galactosidase expression (blue signal) in the white matter and gray matter (see insets). The upper cervical segments (C1) are devoid of recombinase activity. (C) β-galactosidase (green) and neuronal marker NeuN (blue) in superficial dorsal horn of the lumbar spinal cord. Insets are double-positive neurons (black arrowheads) and β-gal-only cells (white arrowheads) (D) Dense tdTomato expression within the spinal cord of *Hoxb8-tdTomato* mice (S, T, L, C7; DsRed+: red signal). In upper cervical segments (C1), axons with DsRed immunoreactivity are primarily observed in white matter tracts (n = 5; 5 sections/animal). (E) These axons are present throughout ascending tracts of (1) dorsal funiculus and (2) lateral funiculus. Scale bar: (B) 250 μm, (C and E) 100 μm; (C inset) 25 μm. ALT, anterolateral tract; cu, cuneate fasciculus; DH, dorsal horn; dcs, dorsal corticospinal tract; LCN, lateral cervical nucleus; psdc, postsynaptic dorsal column; SCT, spinocerebellar tract; VH, ventral horn.

appositions in the parasubthalamic nucleus in the lateral hypothalamus (**Fig. 4L**). These appositions were located adjacent to axon tracts that eventually innervate the globus pallidus (**Fig. 4M**).[13,33,58] Collectively, our results demonstrate that *Hoxb8::Cre* spinal neurons innervate all the major brain regions receiving somatosensory and motor inputs.

3.4. Spinal deletion of Dcc alters spinofugal innervation

We subsequently examined the effect of spinal cord deletion of *Dcc* on the supraspinal connectivity of AS neurons in *Hoxb8::Cre; Dcc$^{flox/-}$* (*Dcc^{SpKO}*) mice. We have previously demonstrated that through this genetic approach, DCC expression is completely lost in the caudal neural tube by E11.5, the time at which many axons cross the ventral spinal commissure. By E14.5, when essentially all commissural axons have crossed the midline, the size of the ventral commissure in *Dcc^{SpKO}* embryos was reduced by approximately 42%,[18] similar to that in mice with constitutive *Dcc* deletion.[28,82] To uncover the changes in the innervation of AS supraspinal targets VPL,[18] PAG, and LPbN, in the absence of DCC, we first labelled these projections anterogradely. We made unilateral lumbar injections of an adeno-associated virus driving the expression of the yellow fluorescent protein citrine (YFP) in presynaptic terminals (AAV2/8-SYP1-miniSOG-citrine) of transduced neurons, in *Dcc^{SpKO}* mice and their control littermates (*Dcc$^{flox/+}$ or Dcc $^{flox/flox}$*) (**Fig. 5A**). In all cases, the transduction was confined to one side of the lumbar spinal cord and generally biased to the SDH where lamina I AS neurons are located but

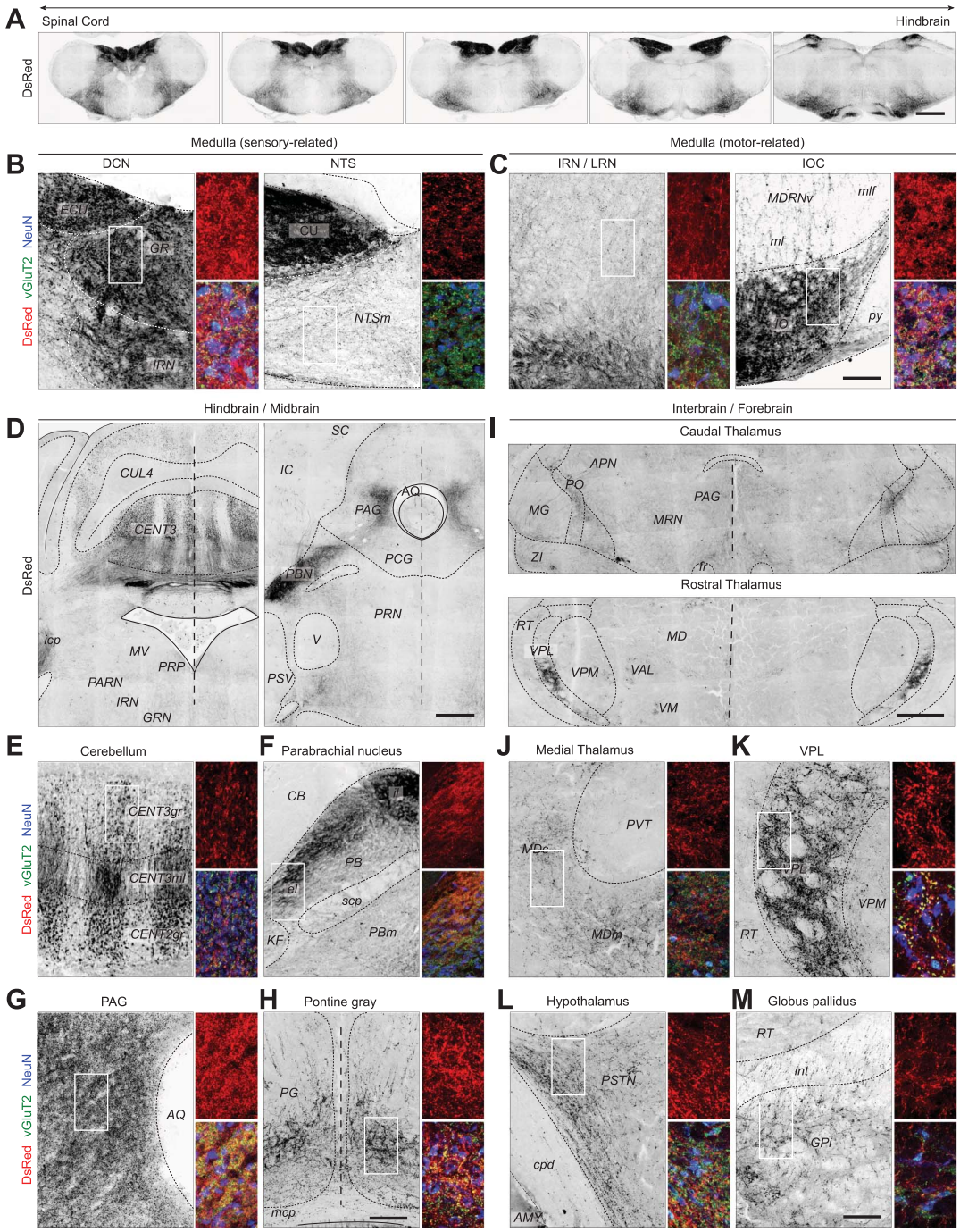

Figure 4. *Hoxb8::Cre* defines genetic access to sensory and motor-related spinofugal neurons. (A) Transverse sections from the medulla in *Hoxb8-tdTomato* mice show extensive axonal innervation (DsRed+) in numerous nuclei associated with both sensory- and motor-related integration. Neurons (NeuN+; blue) of DCN and NTS in the dorsal medulla (B) and IRN/LRN and IOC in the ventral medulla (C) are highly innervated by DsRed+/vGluT2+ (red/green) appositions. (D) Representative transverse sections from rostral hind brain (bregma −6.055 mm) and midbrain (bregma −5.055 mm). Dense innervation of the motor-related regions: cerebellum (E) and pontine gray (H) and sensory-related regions: lateral parabrachial nucleus (F) and periaqueductal gray (G). *Hoxb8-tdTomato* innervation of multiple nuclei in caudal (bregma −2.88) and rostral (bregma −1.55) thalamus (I). Dense innervation of primary targets of spinothalamic neurons: medial thalamus (J) and VPL (K). Lateral hypothalamic nuclei PSTN and ZI (L) and reticulated internal segment of GP (M). (n = 5, 3 sections/animal). Scale bar: (A) 250 μm; (D and J) 500 μm; all others 100 μm. Medulla: CU, cuneate nucleus; DCN, dorsal column nucleus; ECU, external cuneate nucleus; GR, gracile nucleus; GRN, gigantocellular reticular nucleus; IOC, inferior olivary complex; IRN, internal reticular nucleus; LRN, lateral reticular nucleus; MDRNv, medullary reticular nucleus, ventral part; MV, medial vestibular nucleus; NTSm, nucleus of solitary tract, medial part; PARN, parvocellular reticular nucleus; PRP, nucleus prepositus. Pons: PG, pontine gray; PCG, pontine central gray; PRN, pontine reticular nucleus. Cerebellum: CB, cerebellum; CENT2/3: central lobule II/III; CUL4, culmen lobule IV; gr, granular layer; ml, medial layer. Midbrain: APN, anterior pretectal nucleus; AQ, cerebral aqueduct; IC, inferior colliculus; KF, Kölliker–Fuse subnucleus; lc, PBN central lateral part; le, PBN external lateral part; MRN, midbrain reticular nucleus; PAG, periaqueductal gray; PBm, PBN medial part; PBN, parabrachial nucleus; SC, superior colliculus. Thalamus: MD, mediodorsal nucleus; MDc, mediodorsal nucleus, central part; MDm, mediodorsal nucleus, medial part; MG, medial geniculate complex; PO, posterior complex; PVT, paraventricular nucleus; RT, reticular nucleus of the thalamus; SPFp, subparafascicular nucleus, paracellular part; VAL, ventral anterior–lateral complex; VM, ventral medial nucleus; VPL, ventral posteromedial nucleus; VPM, ventral posteromedial nucleus. Hypothalamus: PTSN, parasubthalamic nucleus; ZI, zona incerta. Cerebral cortex: AMY, amygdala; GPi, globus pallidus, internal segment. Fibre tracts: *cpd*, cerebral peduncle; *fr*, fasciculus retroflexus; *icp*, inferior cerebellar peduncle; *int*, internal capsule; *mcp*, middle cerebellar peduncle; *ml*, medial lemniscus; *mlf*, medial longitudinal fascicle; *py*, pyramidal tract; *scp*, superior cerebellar peduncle.

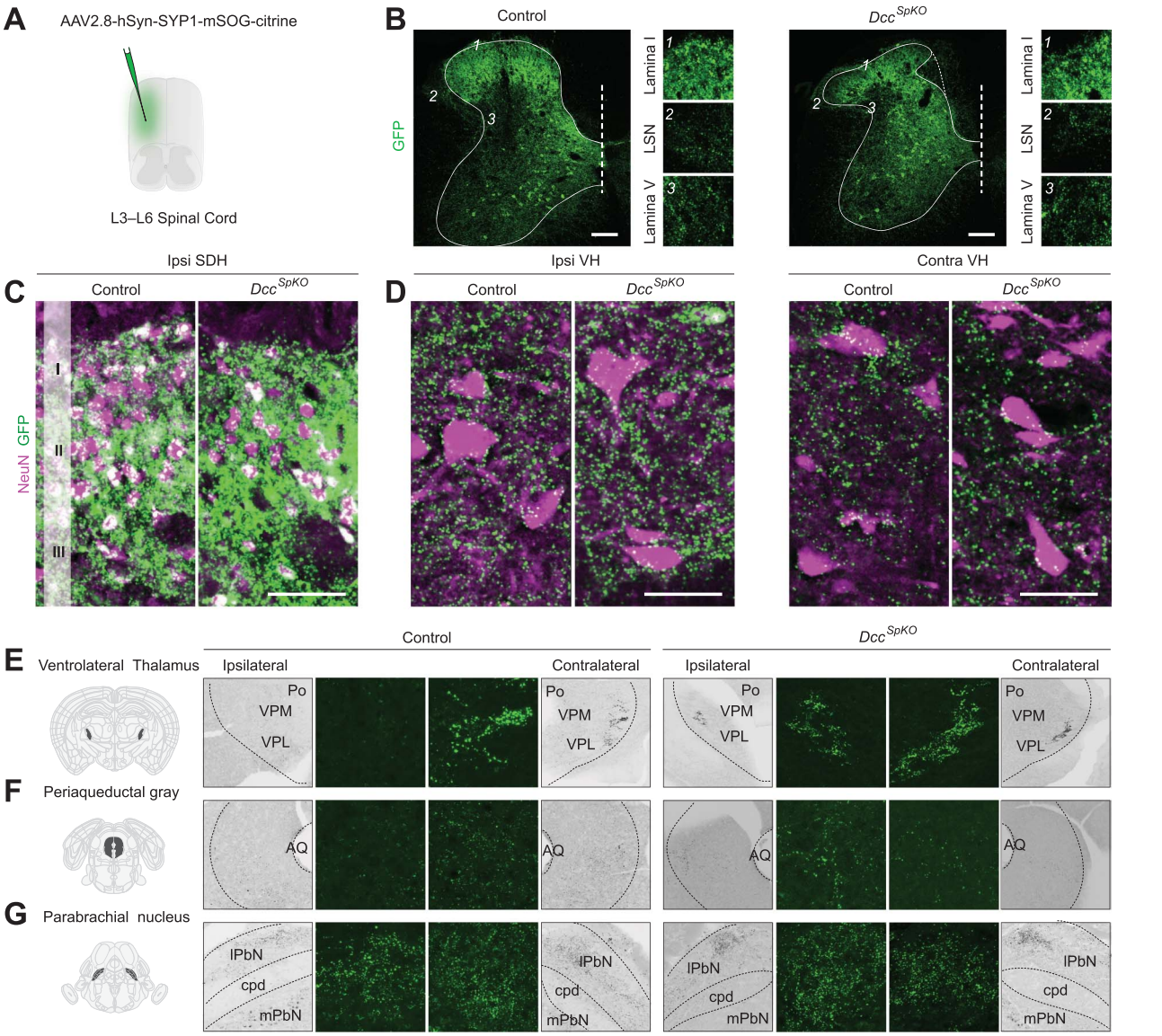

Figure 5. Viral anterograde labelling of AS axons reveals a shift in laterality in Dcc^{SpkO}. (A) Schematic of the unilateral injections of AAV2/8-hSyn-SYP1-miniSOG-Citrine in the lumbar enlargement. (B) Representative transverse images showing YFP expression restricted to one side of the lumbar spinal cord in control and *Dcc*^{SpkO} mice. YFP+ synaptic terminals are largely enriched in the superficial dorsal horn (C) and more sparsely in the ipsilateral and contralateral ventral horn (D) of control and *Dcc*^{SpkO} mice. YFP+ spinofugal neuron axon terminals are primarily contralateral in the VPL thalamus (E) and PAG (F) in control mice. In *Dcc*^{SpkO} mice, spinofugal projections appear bilateral in VPL and PAG (E and F). Spinoparabrachial neuron axon terminals seem to innervate the LPbN bilaterally in both control and *Dcc*^{SpkO} (G). (n = 3/genotype, 3 sections/animal). Scale bar: (C and D) 25 μm, (B and E–G) 100 μm; (E–G inset) 25 μm. AQ, cerebral aqueduct; AS, anterolateral system; AAV, adeno-associated virus; CBX, cerebellar cortex; IC, inferior colliculus; LPbN, lateral parabrachial nucleus; PAG, periaqueductal gray; PBN, parabrachial nucleus; PCG, pontine central gray; PRN, pontine reticular nucleus; PSV, principal sensory trigeminal nucleus; VPL, ventral posterolateral.

excluding those in lamina V or LSN (**Figs. 5B and C**). We detected some YFP+ synaptic terminals in the LSN in agreement with propriospinal peptidergic inputs to this region.[14,35] Citrine-expressing (YFP+) appositions were detectable in both ipsilateral and contralateral ventral horn neurons (**Fig. 5D**) in *Dcc*^{SpKO} and control lumbar spinal cords, most likely from local interneurons.[3,32] We also observed a change in the morphology of the dorsal horn of *Dcc*^{SpKO} mice (**Fig. 5B** dashed region), similar to that previously seen in constitutive *Dcc* mutants[8,22,28]: dorsal white matter area appeared increased and the medial portion of the dorsal horn appeared highly reticulated compared to control littermates. We then examined the VPL, LPbN, and PAG of both injected groups, to qualitatively assess AS spinofugal innervation. The distributions of the AS spinofugal axons in the thalamus were consistent with our previous report[18] where we demonstrated that ST neurons in *Dcc*^{SpKO} project bilaterally to the thalamus using retrograde labeling. Here, although dense YFP-expressing axons were exclusively detected in the contralateral VPL in control mice, we observed dense appositions in *Dcc*^{SpKO} on both ipsilateral and contralateral lobes of the lateral thalamus in *Dcc*^{SpKO} mice (**Fig. 5E**). Similarly, in the midbrain, although control animals had very sparse labelling in the ipsilateral PAG, we detected an increased presence of YFP+ terminals in the ipsilateral PAG of *Dcc*^{SpKO} mice (**Fig. 5F**). By contrast, given that the LPbN receives bilateral innervation,[72] we observed similar labelling bilaterally in both control and *Dcc*^{SpKO} mice (**Fig. 5G**). Together, these results suggest that the loss of DCC expression during the formation of spinal commissural circuits alters the lateralization of AS axon terminals at their supraspinal targets.

3.5. Laterality changes in lamina I but not lamina V or lateral spinal nucleus anterolateral system neurons

Despite this apparent shift in laterality of anterogradely labelled spinofugal axons in Dcc^{SpKO} mutants, a bias in viral transduction favouring the SDH impeded a thorough assessment of the impact of deletion of *Dcc* in the major AS clusters in lateral lamina V and LSN (**Fig. 5B**, insets). To accurately assess the changes in laterality of most AS neuronal projections caused by the loss of DCC, we made a unilateral injection of the retrograde fluorescent tracer CTB conjugated to Alexa Fluor 488 in the LPbN of Dcc^{SpKO} and their control littermates, and examined the distribution of SPb (spinoparabrachial) neurons in the lumbar enlargement (**Fig. 6A**). In all experimental animals, the injected CTB was largely restricted to the LPbN (**Fig. 6B**). In agreement with previous studies,[41,46,56] CTB-labelled neurons were largely found in lamina I, lateral lamina V, and the LSN of the dorsal horn in both control and Dcc^{SpKO} mice (**Figs. 6C and D**). We quantified 156 ± 56.6 SPb neurons from 10 transverse sections per animal (both ipsilateral and contralateral in 25-μm sections). These neurons were subdivided into 3 main clusters: SDH (lamina I), DDH (lamina III-V), and the LSN. We plotted the relative position of both ipsilateral and contralateral neurons (**Figs. 6E and F**) using the central canal as the reference point.[76] SPb neurons in the SDH were predominantly found in the contralateral lumbar cord in control mice. By contrast, in the Dcc^{SpKO}, many SDH neurons were visible in the ipsilateral spinal cord. SPb neurons in the LSN and DDH seemed to be present bilaterally in both groups. In the DDH of Dcc^{SpKO} mice, however, SPb neurons seemed to be more broadly distributed throughout the gray matter (**Fig. 6F**). We examined the ratio of contralateral to ipsilateral neurons (C/I ratio) in each group to determine whether the impact of *Dcc* deletion affects the connectivity of SPb clusters differentially (**Fig. 6G** and **Table 2**). In control mice, most SDH SPb neurons projected contralaterally (contra 85.9% vs ipsi 14.1% ± 3.4%; C/I ratio of 10.53 ± 5.19). There were no apparent laterality biases in DDH (contra 46.64% vs ipsi 53.37% ± 4.1%; C/I ratio of 0.92 ± 0.15) or LSN neurons (contra 56.20% vs ipsi 43.8% ± 2.4%; C/I ratio of 1.31 ± 0.13), suggesting that SPb neurons are bilaterally distributed in the DDH and the LSN. By contrast, in Dcc^{SpKO} mice, SPb neurons in the SDH were equally distributed between the ipsilateral and contralateral spinal cord (contra 50.11% vs ipsi 49.89% ± 1.9%; C/I ratio of 1.01 ± 0.07). When comparing the contralateral % of SPb neurons in SDH between mutant and control groups, we found it significantly different (Mann–Whitney test, $P = 0.0159$). However, such analyses indicated no changes in the apparent percent laterality of DDH-SPb neurons ($P = 0.7302$) or LSN-SPb projections ($P = 0.2857$). Previous work has demonstrated that DCC expression is essential for the appropriate migration of spinal neurons.[22] We therefore assessed potential changes to the mediolateral distribution of labelled SPb neurons using density plots representing multiple sections (**Fig. 6H**). We compared the mean mediolateral distance of labelled neurons between control and Dcc^{SpKO} mice on both the contralateral and ipsilateral spinal cord. The mediolateral distribution of all clusters remained unchanged in Dcc^{SpKO} mice (Mann–Whitney test, control vs Dcc^{SpK} SDH: 576.8 ± 16.4 vs 614.5 ± 22.9 μm, $P = 0.3154$; LSN; 838.1 ± 13.8 vs 862.4 ± 13.4 μm, $P = 0.2115$; DDH: 562.7 ± 41.7 vs 488.5 ± 47.9, $P = 0.1365$).

We subsequently examined the distribution of AS neurons innervating the PAG (spinoperiaqueductal gray; SPAG) through a similar retrograde labeling approach (**Fig. 7A**). The injection of CTB-488 was entirely restricted to one side of the PAG (**Fig. 7B**). We then quantified 144.9 ± 20.3 labelled neurons from 10 transverse sections per animal (both ipsilateral and contralateral in 25-μm sections). Similar to SPb neuron distribution, SPAG neurons were primarily confined to the SDH, LSN, and DDH regions[6,51,55] in both control and Dcc^{SpKO} mice (**Figs. 7C–F**). Through our cluster analysis (**Fig. 7G** and **Table 3**), we observed that the contralaterally biased SDH neurons in control mice (contra 79.6% vs ipsi 20.4% ± 6.0%; C/I ratio of 3.91 ± 2.99) demonstrated a shift toward projecting ipsilaterally in Dcc^{SpKO} mice (contra 46.2% vs ipsi 53.8% ± 4.7%; C/I ratio of 0.86 ± 0.19) (Mann–Whitney comparing contra % in controls vs mutants; $P = 0.0286$). The SPb and SPAG neurons in the SDH were entirely confined to lamina I of Rexed.[66,71] The broad distribution of these cells in **Figures 6E and 7E**, however, seems due to changes in the general shape of the dorsal horn from the examined cross-section. However, the laterality of LSN (Control: contra 52.1% vs ipsi 47.9% ± 1.9%; C/I ratio of 1.09 ± 0.08; Dcc^{SpKO}: contra 52.9% vs 47.1% ± 4.0%; C/I ratio of 1.12 ± 0.21) and DDH (Control: contra 53.2% vs ipsi 46.8% ± 4.9%; C/I ratio of 1.1 ± 0.21; Dcc^{SpKO}: contra 52.1% vs 47.2% ± 1.6%; C/I ratio of 1.09 ± 0.07) neurons, already projecting evenly to both sides, did not change (Mann–Whitney, $P = 0.8857$ and 0.4857, respectively). Comparing the distribution of the labelled neurons, no significant mediolateral differences were evident between control Dcc^{SpKO} mice (**Fig. 7H**). Together, these results suggest that lamina I AS neurons profoundly rely on DCC for targeting to their respective supraspinal targets during development; however, the mediolateral position of AS neurons seems unaffected in the absence of DCC.

4. Discussion

Together, our experiments provide a detailed overview of *Hoxb8::Cre* expression in spinofugal neurons, and further demonstrate their dependence on DCC during development. Here, we discuss our findings in terms of AS ontogeny, anatomy of ascending sensory and motor pathways, and the potential role of AS connection topography in nociception.

Hoxb8::Cre is expressed in all spinal progenitors as early as E9.5, apparently preceding the birth time of many AS neurons.[59] It is expressed in cardinal commissural spinal neuron populations (dI1, dI5, or V3) that likely give rise to excitatory spinofugal neurons, including those of the AS. However, more generally, the *Hoxb8::Cre* characterization study by Witschi et al.[81] reported a slightly higher fraction of spinal neurons that express *Hoxb8::Cre* (96.0% ± 0.8 vs our 88.9% ± 1.35). This may be explained by the nuclear LacZ reporter allowing us to resolve *Hoxb8::Cre* expression at the level of individual cells, without the confound of cellular Cre reporter signal in dense neurites in the spinal dorsal horn. In addition, using 2 separate Cre-dependent reporters, we were unable to detect any *Hoxb8::Cre* recombinase expression in the neurons of the spinal trigeminal nucleus or their axon terminals in the ventral posteromedial thalamus, previously shown by Witschi et al.[81] Because we detected microglial *Hoxb8::Cre* expression in the rostral nervous system, including the brainstem, the previously identified *Hoxb8::Cre* expression in the trigeminal nucleus may have been nonneuronal. Given these observations, we conclude that *Hoxb8::Cre* drives recombination in the spinal cord while essentially sparing the brain.

We also demonstrate that *Hoxb8::Cre* is expressed in sensory and motor spinofugal neurons that innervate the brainstem and the forebrain. One limitation of the *Hoxb8::Cre* line is that it spares all spinofugal neurons positioned in the upper cervical spinal cord. Because this region contains numerous neurons that contribute

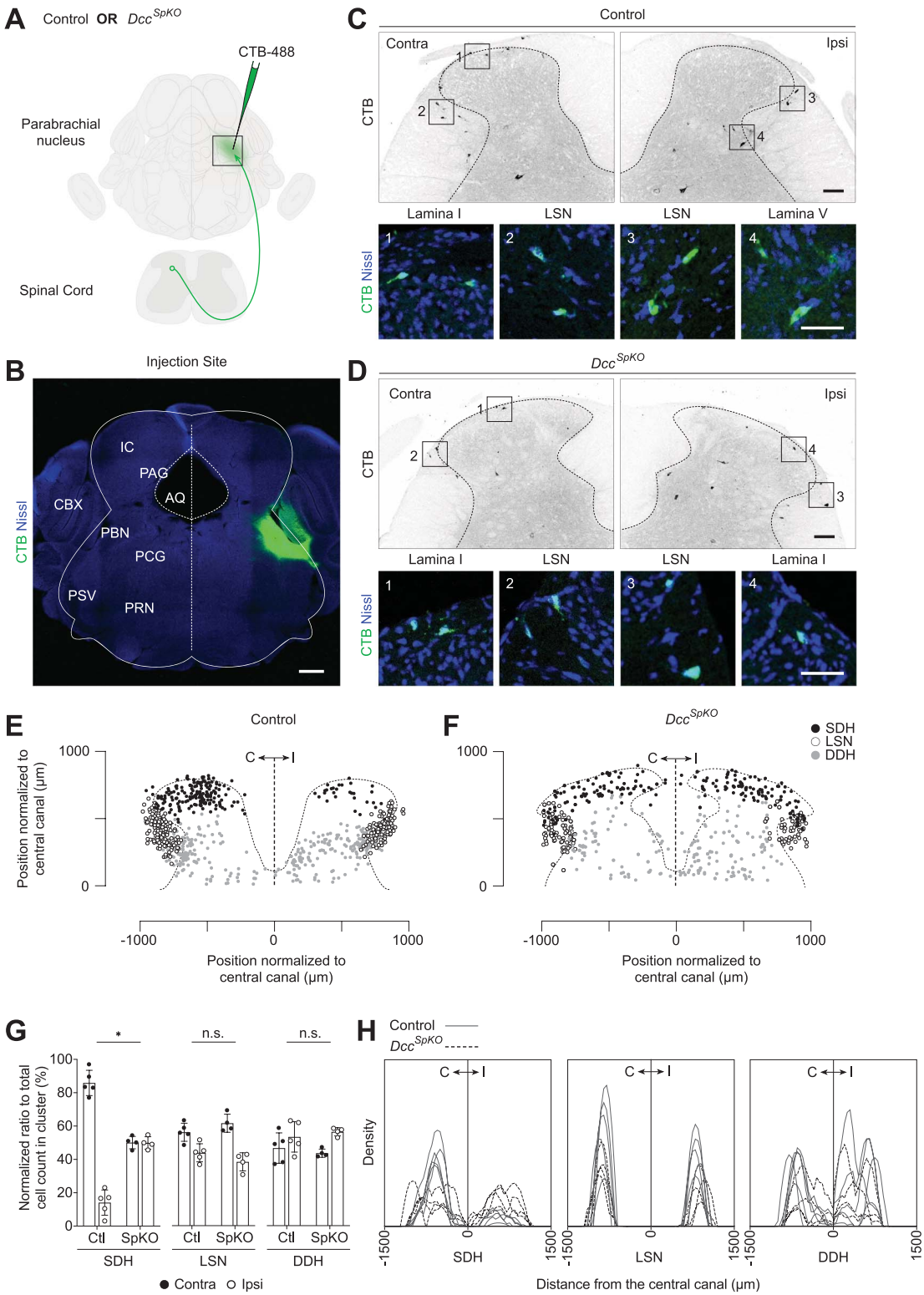

Figure 6. Retrograde labelling reveals a shift in the laterality of multiple spinoparabrachial neuron populations in *Dcc*^{SpkO}. (A) Schematic of unilateral retrograde labelling of SPb neurons in control and *Dcc*^{SpkO} mice. (B) Representative confocal image of CTB-488 (green) injection restricted to the LPbN (tissue counterstained with blue fluorescent Nissl stain). Images from the ipsilaterally and contralaterally labelled SPb neurons (top row: CTB+ neurons in black) in the spinal lumbar enlargement in (C) control mice and (D) *Dcc*^{SpkO}. Bottom row: Micrographs of CTB+ (green) projection neurons in lamina I, V, and LSN. Relative position of identified SPb neurons in SDH (black), LSN (white), and DDH (gray) in the lumbar spinal cord in (E) control and (F) *Dcc*^{SpkO} mice. (G) The relative ratio of all (SDH, LSN, and DDH) identified ipsilateral (white) and contralateral (black) labelled SPb neurons in control and *Dcc*^{SpkO} mice. (H) Density of plots of the relative mediolateral position of labelled SPb neurons in the spinal cord of control (solid) and *Dcc*^{SpkO} (dashed) mice. (n = 5 for control and n = 4 for *Dcc*^{SpkO}; 10 sections/side/animal; $^{**}P < 0.001$, $^{*}P < 0.01$; Mann–Whitney test). Scale bar: (B) 500 μm, (C and D) 100 μm; (C and D inset) 25 μm; (C) 100 μm, (inset) 25 μm. AQ, cerebral aqueduct; CBX, cerebellar cortex; DDH, deep dorsal horn; IC, inferior colliculus; LPbN, lateral parabrachial nucleus; LSN, lateral spinal nucleus; PAG, periaqueductal gray; PBN, parabrachial nucleus; POR, periolivary region (superior olivary complex); PRN, pontine reticular nucleus; PSV, principal sensory trigeminal; SC, superior colliculus; SDH, superficial dorsal horn.

Table 2

Quantitative assessment of laterality changes in the innervation of lateral parabrachial nucleus by the AS neurons represented as percent ratios of retrogradely labelled AS neurons.

Mouse	SPb									
	Control (n = 5)					*Dcc*^{SpKO} (n = 4)				
	No. of cells		Percentage (%)		Ratio (C/I)	No. of cells		Percentage (%)		Ratio (C/I)
	Contra	Ipsi	Contra	Ipsi		Contra	Ipsi	Contra	Ipsi	
SDH										
1	30	9	76.92	23.08	3.33	28	27	50.91	49.09	1.04
2	51	6	89.47	10.53	8.5	19	23	45.24	54.76	0.83
3	29	6	82.86	17.14	4.83	19	16	54.29	45.71	1.19
4	31	1	96.88	3.13	31	35	35	50	50	1
5	35	7	83.33	16.67	5					
Mean			85.89	14.11	10.53			50.11	49.89	1.01
SEM			3.39		5.19			1.87		0.07
LSN										
1	15	16	48.39	51.61	0.94	18	8	69.23	30.77	2.25
2	39	32	54.93	45.07	1.22	20	15	57.14	42.86	1.33
3	43	25	63.24	36.76	1.72	21	13	61.76	38.24	1.62
4	27	19	58.7	41.3	1.42	28	20	58.33	41.67	1.4
5	34	27	55.74	44.26	1.26					
Mean			56.2	43.8	1.31			61.62	38.38	1.65
SEM			2.44		0.13			2.72		0.21
DDH										
1	17	12	58.62	41.38	1.42	8	9	47.06	52.94	0.89
2	31	53	36.9	63.1	0.58	11	15	42.31	57.69	0.73
3	35	57	38.04	61.96	0.61	17	24	41.46	58.54	0.71
4	23	24	48.94	51.06	0.96	43	56	43.43	56.57	0.77
5	38	37	50.67	49.33	1.03					
Mean			46.63	53.37	0.92			43.57	56.43	0.77
SEM			4.09		0.15			1.23		0.04

AS, anterolateral system; DDH, deep dorsal horn; LSN, lateral spinal nucleus; SDH, superficial dorsal horn.

to ascending sensory tracts in rodents,[5] our axonal reporter characterization in the brain is therefore an underrepresentation of all spinofugal axons terminals. Nevertheless, our analysis provides the first large-scale description of all caudal spinofugal inputs in the mouse brain. A previous low-resolution study showed that *Cdx1::Cre,* expressed in the caudal spinal cord, labels spinofugal axons tracts in the prenatal mouse brain.[39] Our analysis, however, provides a more comprehensive analysis of all spinofugal connections and is combined with the visualization of presynaptic markers in the adult mouse brain, which distinguishes passing axons from axonal termini. In contrast to other mammalian spinofugal projection mapping using classic anterograde labels,[9,13,44,58] we found no spinofugal axon terminals in the medial hypothalamus. Because spinohypothalamic neurons are present throughout the rostrocaudal extent of the spinal cord, including in the lumbar region, the presence of *Hoxb8::Cre*-expressing axons in the medial hypothalamus should have been apparent. The lack of such axon terminals in the mouse suggests that the innervation pattern of ascending tracts may not necessarily be phylogenically conserved.

Our quantitative experiments also allow some insights into the lateralization of AS projections in the absence of Netrin-1:DCC signalling during spinal cord development. The laterality of AS axons in the LSN and DDH is largely unaffected by the *Dcc*^{SpKO} mutation. This is in line with apparently similar proportions of contralateral and ipsilateral axon terminals in the LPbN and PAG, as revealed by single tracer injections in the lamina V/LSN lumbar region.[7] In addition, ipsilateral DDH SPb neurons are also present throughout the spinal cord, although in smaller numbers than contralateral neurons.[46] Thus, because many LSN and DDH axons do not cross the spinal midline, this aspect of their connectivity is likely to be DCC-independent and may involve other midline crossing mechanisms. Another technical caveat to consider is that the LPbN is adjacent to the ventral spinocerebellar tract that originates from a large population of ipsilateral spinocerebellar neurons found throughout the lumbar DDH.[53,54] Given the proximity of the LPbN injection site to the cerebellum, it is likely that the CTB-labelled neurons found in the DDH of both control and *Dcc*^{SpKO} mice may include some spinocerebellar neurons.

The most pronounced AS connectivity change in *Dcc*^{SpKO} mice was in the laterality of SDH AS neurons where significantly more of them were innervating their targets on the ipsilateral side. Previous work in rats demonstrates that lumbar lamina I SPb neurons are mostly contralateral, whereas a third project bilaterally.[72] The increase in the proportion of ipsilateral projections in *Dcc*^{SpKO} is consistent with the bilaterally projecting SPb neurons either losing their midline crossing (ie, contralateral) axon such that only the ipsilateral projection remains, or with the contralateral axons ascending alongside their ipsilateral collateral. However, due to the variability in the absolute numbers of labelled SPb neurons, we are unable to resolve between these 2 possibilities. Consistent with previous reports that virtually all lamina I SPAG also innervate the LPbN,[72] we observed this laterality change when assessing SDH AS neuronal projections to the PAG and LPbN. This is reminiscent of observations made in *Krox20:Cre; Robo3*$^{flox/flox}$ (*Robo3*$^{R3\text{-}5}$*cKO*) mice in which trigeminothalamic neurons lack Robo3, another important commissural

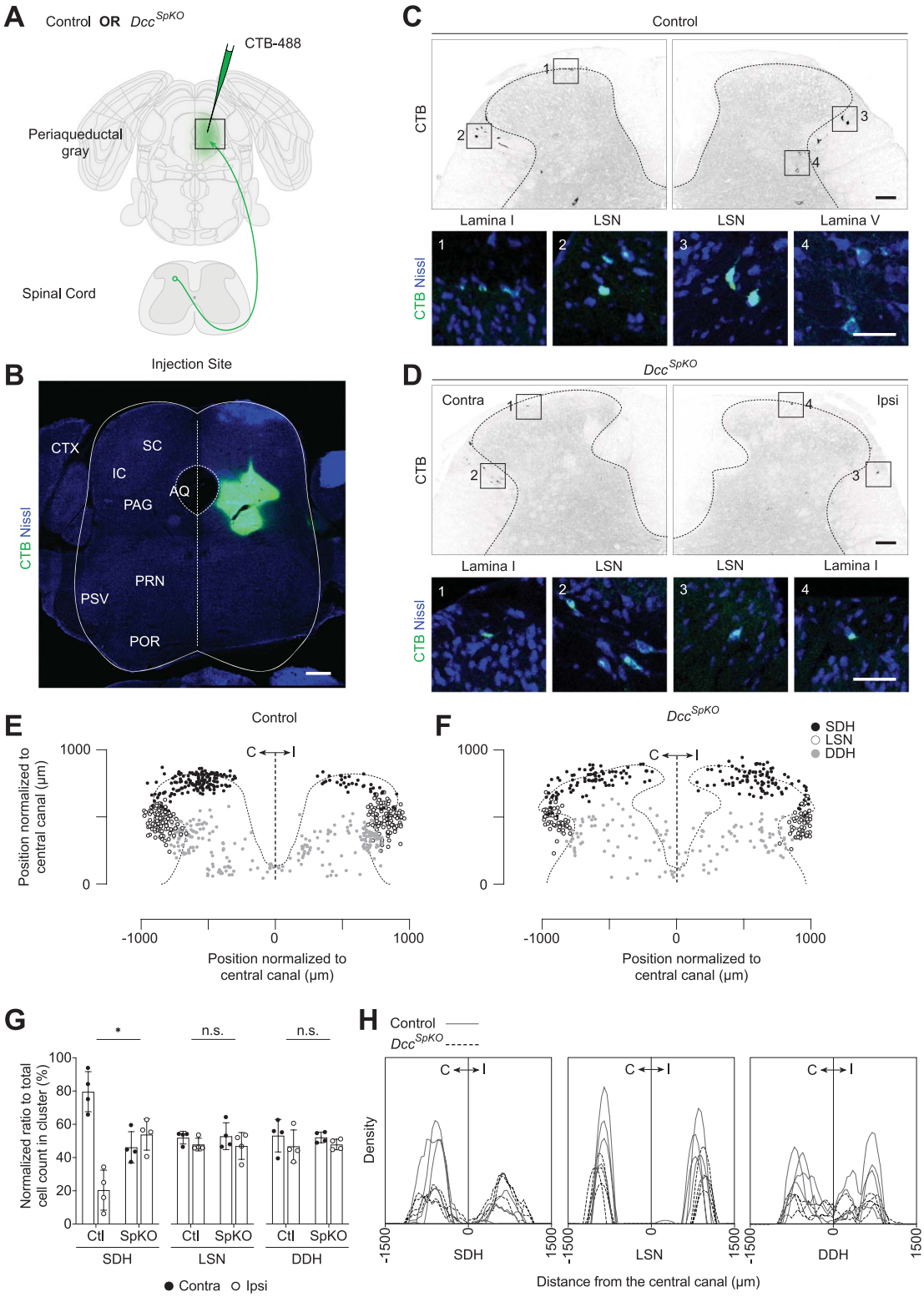

Figure 7. Retrograde labelling reveals an increase in ipsilateral projections of lamina I spinoperiaqueductal gray (SPAG) neurons in *Dcc*^{SpkO}. (A) Schematic of unilateral retrograde labelling of SPAG neurons in control and *Dcc*^{SpkO} mice. (B) Representative confocal image of CTB-488 (green) injection restricted to the PAG (tissue counterstained with blue fluorescent Nissl stain). Images from the ipsilaterally and contralaterally labelled SPAG neurons (top row: CTB+ neurons in black) in the spinal lumbar enlargement in (C) control mice and (D) *Dcc*^{SpkO}. Bottom row: Micrographs of CTB+ (green) projection neurons in lamina I, V, and LSN. Relative position of identified SPAG neurons in SDH (black), LSN (white), and DDH (gray) in the lumbar spinal cord in (E) control and (F) *Dcc*^{SpkO} mice. (G) The relative ratio of all (SDH, LSN, and DDH) identified ipsilateral (white) and contralateral (black) labelled SPb neurons in control and *Dcc*^{SpkO} mice. (H) Density of plots of the relative mediolateral position of labelled SPb neurons in the spinal cord of control (solid) and *Dcc*^{SpkO} (dashed) mice. (n = 4 for each group; 10 sections/side/animal; $^{**}P < 0.001$, $^{*}P < 0.01$; Mann–Whitney test). Scale bar: (B) 500 μm, (C and D) 100 μm; (C and D inset) 25 μm; (C) 100 μm, (inset) 25 μm. AQ, cerebral aqueduct; CBX, cerebellar cortex; CTB, cholera toxin B; DDH, deep dorsal horn; IC, inferior colliculus; LSN, lateral spinal nucleus; PAG, periaqueductal gray; PBN, parabrachial nucleus; POR, periolivary region (superior olivary complex); PRN, pontine reticular nucleus; PSV, principal sensory trigeminal; SC, superior colliculus; SDH, superficial dorsal horn.

Table 3

Quantitative assessment of laterality changes in the innervation of periaqueductal gray by the AS neurons represented as percent ratios of retrogradely labelled AS neurons.

Mouse	SPAG									
	Control (n = 5)					Dcc^{SpKO} (n = 4)				
	No. of cells		Percentage (%)		Ratio (C/I)	No. of cells		Percentage (%)		Ratio (C/I)
	Contra	Ipsi	Contra	Ipsi		Contra	Ipsi	Contra	Ipsi	
SDH										
1	30	10	75.00	25.00	3.00	19	13	59.38	40.63	1.46
2	44	23	65.67	34.33	1.91	23	30	43.40	56.60	0.77
3	58	11	84.06	15.94	5.27	25	31	44.64	55.36	0.81
4	15	1	93.75	6.25	15.00	16	27	37.21	62.79	0.59
Mean			79.62	20.38	3.91			46.16	53.84	0.86
SEM			6.02		2.99			4.69		0.19
LSN										
1	26	22	54.17	45.83	1.18	13	15	46.43	53.57	0.87
2	44	38	53.66	46.34	1.16	17	15	53.13	46.88	1.13
3	33	28	54.10	45.90	1.18	23	25	47.92	52.08	0.92
4	19	22	46.34	53.66	0.86	18	10	64.29	35.71	1.80
Mean			52.07	47.93	1.09			52.94	47.06	1.12
SEM			1.91		0.08			4.05		0.21
DDH										
1	29	23	55.77	44.23	1.26	18	15	54.55	45.45	1.20
2	37	57	39.36	60.64	0.65	20	20	50.00	50.00	1.00
3	38	31	55.07	44.93	1.23	20	21	48.78	51.22	0.95
4	20	12	62.50	37.50	1.67	16	13	55.17	44.83	1.23
Mean			53.18	46.82	1.14			52.12	47.88	1.09
SEM			4.90		0.21			1.60		0.07

AS, anterolateral system; DDH, deep dorsal horn; LSN, lateral spinal nucleus; SDH, superficial dorsal horn; SPAG, spinoperiaqueductal gray.

crossing receptor. In these mice, the number of contralateral trigeminothalamic connections was decreased, with a concomitant increase in ipsilateral ones, suggesting that a ventral posteromedial thalamus lobe on one side of the thalamus receives whisker inputs from trigeminal neurons on both sides of the body.[65] We thus envisage that a similar input convergence may occur in SDH AS neuron innervation of their targets in Dcc^{SpKO} mice. Although *Dcc* loss increased the number of ipsilateral SDH AS neurons, a considerable number of them formed contralateral connections suggesting that Nerin1:DCC signalling may be dispensable for their commissural crossing. Complete loss of Netrin-1 or DCC is associated with a reduction but not a total loss of ventral commissures.[8,18,82] Remarkably, combined deletion of DCC and Neogenin1, also a Netrin-1 receptor, generates a near absence of the ventral commissure[82] suggesting that Netrin-1 may exert some of its chemoattraction through a DCC-independent mechanism. All commissural neurons of the spinal cord also express Robo3.[11,31,69,77] Although developmental deletion of *Dcc* reduces ventral commissural crossing, the loss of *Robo3* expression completely eliminates the ventral crossing.[42,69] These findings collectively suggest that although DCC is important for the commissural guidance, other molecules have been found to make important contributions to it.

What is the consequence of AS neurons from both sides of the spinal cord innervating a target on one side of the nervous system? Most lateralized neural circuits are somatotopically organized where adjacent projection neurons innervate adjacent regions of the target, forming classic somatotopically ordered maps. In $Robo3^{R3\text{-}5}cKO$ mice, the axon terminals originating from left or right side of the trigeminal nucleus segregated into separate domains within one thalamic lobe, such that left and right side trigeminothalamic axons innervated separate thalamic neurons within a thalamic lobe.[65] Similar observations were made in monkey ocular dominance columns[40] or retinotectal input segregation in three-eyed frogs.[15] Such aberrant trigeminothalamic maps are the likely cause of the decreased accuracy of somatosensory function, inferred from aberrant whisker-dependent behaviors observed in $Robo3^{R3\text{-}5}cKO$ mice. Anterolateral system neurons are also somatotopically organized, where, for example, spinothalamic AS neurons from the caudal spinal cord innervate the lateral edge of the VPL, whereas those in the cervical spinal cord terminate more medially.[30] To determine whether SDH neuron targeting in Dcc^{SpKO} mice results in somatotopic shifts similar to those in $Robo3^{R3\text{-}5}cKO$ mutants, it is imperative to label projections from each side of the superficial spinal cord and examine the somatotopic organization of axon terminals in each of the primary targets (ie,: VPL, PAG, and LPbN) in the brain. However, such an experiment is limited by the small number of spinothalamic neurons in the caudal spinal cord. Despite this limitation, given the somatotopic organization of nociceptive DDH neurons, and a similar arrangement of their VPL thalamus targets, we propose that the decreased laterality of DDH-VPL connections may contribute to the inaccurate localization (topognosis) of painful stimuli in Dcc^{SpKO} mice.

Could other AS targets be contributing to nociceptive topognosis? A major component of nociception is the rapid generation of a defense vs escape response, facilitated primarily by neurons in the PAG.[20,27] In the case of escape, for example, accurate localization of the stimulus may dictate the direction of escape. The contralateral lamina I spinofugal inputs to the PAG (in addition to VPL thalamus) may contribute to such responses. Direct activation of lateral PAG in cats and rats elicit both a somatotopically organized and asymmetrical defense response.

Microinjection of excitatory amino acids or direct electrical stimulation in the PAG in conjunction with facial tactile stimulation elicits fight responses with the head moving to the contralateral side.[4] Although the activation of the pretentorial PAG evokes threat displays towards the contralateral facial and forelimbs regions, the activation of the subtentorial PAG results in flight reactions associated with hind limb movement.[21] Recent findings also illustrate that direct inputs from the LPbN to LPAG are associated with driving escape behaviours in mice,[12] raising the possibility that lateralized lamina I inputs in the LPbN may be necessary to drive appropriate cross-talk between LPbN and LPAG. Consequently, an increase in lamina I AS neuron ipsilateral connectivity to the PAG may also contribute to the aberrant nocifensive response to noxious stimuli found in *Dcc*^{SpKO} mice.

Conflict of interest statement

The authors have no conflicts of interest to declare.

Acknowledgements

The authors thank Isobel Orfi and Wren Boehlen for assistance in tissue processing and image acquisition; Meirong Liang and Julie Cardin for genotyping of transgenic mice; Carmen Birchmeier and Thomas Müller for providing the Lmx1b antibody; and R. Brian Roome, Shannon Swikert, and Chao Chang for comments and feedback on the manuscript.
This work was supported by Canadian Institutes of Health Research (grants PJT-153053, PJT-159839, and PJT-162225), Brain Canada, Canadian Foundation for Innovation, and the W. Garfield Weston Foundation.

Article history:
Received 27 March 2020
Received in revised form 8 July 2020
Accepted 13 July 2020
Available online 21 July 2020

References

[1] Al-Khater KM, Kerr R, Todd AJ. A quantitative study of spinothalamic neurons in laminae I, III, and IV in lumbar and cervical segments of the rat spinal cord. J Comp Neurol 2008;511:1–18.
[2] Andrew D, Craig AD. Spinothalamic lamina I neurons selectively sensitive to histamine: a central neural pathway for itch. Nature Neuroscience 2001;4:72–7.
[3] Arber S. Motor circuits in action: specification, connectivity, and function. Neuron 2012;74:975–89.
[4] Bandler R, Carrive P. Integrated defence reaction elicited by excitatory amino acid microinjection in the midbrain periaqueductal grey region of the unrestrained cat. Brain Res 1988;439:95–106.
[5] Basbaum AI, Bushnell MC. Science of pain. Academic Press, 2008.
[6] Beitz AJ. The organization of afferent projections to the midbrain periaqueductal gray of the rat. Neuroscience 1982;7:133–59.
[7] Bernard JF, Dallel R, Raboisson P, Villanueva L, Le Bars D. Organization of the efferent projections from the spinal cervical enlargement to the parabrachial area and periaqueductal gray: a PHA-L study in the rat. J Comp Neurol 1995;353:480–505.
[8] Bin JM, Han D, Sun KLW, Croteau LP, Dumontier E, Cloutier JF, Kania A, Kennedy TE. Complete loss of netrin-1 results in embryonic lethality and severe axon guidance defects without increased neural cell death. Cell Rep 2015;12:1099–106.
[9] Burstein R, Cliffer KD, Giesler GJ. Cells of origin of the spinohypothalamic tract in the rat. J Comp Neurol 1990;291:329–44.
[10] Chen SK, Tvrdik P, Peden E, Cho S, Wu S, Spangrude G, Capecchi MR. Hematopoietic origin of pathological grooming in Hoxb8 mutant mice. Cell 2010;141:775–85.
[11] Chédotal A. Roles of axon guidance molecules in neuronal wiring in the developing spinal cord. Nat Rev Neurosci 2019;20:1–17.
[12] Chiang MC, Nguyen EK, Canto-Bustos M, Papale AE, Oswald AMM, Ross SE. Divergent neural pathways emanating from the lateral parabrachial nucleus mediate distinct components of the pain response. Neuron 2020;106:927–39.e5.
[13] Cliffer KD, Burstein R, Giesler GJ. Distributions of spinothalamic, spinohypothalamic, and spinotelencephalic fibers revealed by anterograde transport of PHA-L in rats. J Neurosci 1991;11:852–68.
[14] Cliffer KD, Urca G, Elde RP, Giesler GJ. Studies of peptidergic input to the lateral spinal nucleus. Brain Res 1988;460:356–60.
[15] Constantine-Paton M, Law MI. Eye-specific termination bands in tecta of three-eyed frogs. Science 1978;202:639–41.
[16] Craig AD, Serrano LP. Effects of systemic morphine on lamina I spinothalamic tract neurons in the cat. Brain Res 1994;636:233–44.
[17] Craig ADB. Pain mechanisms: labeled lines versus convergence in central processing. Annu Rev Neurosci 2003;26:1–30.
[18] da Silva RV, Johannssen HC, Wyss MT, Roome RB, Bourojeni FB, Stifani N, Marsh APL, Ryan MM, Lockhart PJ, Leventer RJ, Richards LJ, Rosenblatt B, Srour M, Weber B, Zeilhofer HU, Kania A. DCC is required for the development of nociceptive topognosis in mice and humans. Cell Rep 2018;22:1105–14.
[19] Davidson S, Truong H, Giesler GJ Jr. Quantitative analysis of spinothalamic tract neurons in adult and developing mouse. J Comp Neurol 2010;518:3193–204.
[20] Depaulis A, Bandler R. The midbrain periaqueductal gray matter: functional, anatomical, and neurochemical organization. Springer US, 2012.
[21] Depaulis A, Bandler R, Vergnes M. Characterization of pretentorial periaqueductal gray matter neurons mediating intraspecific defensive behaviors in the rat by microinjections of kainic acid. Brain Res 1989;486: 121–32.
[22] Ding YQ. Ventral migration of early-born neurons requires Dcc and is essential for the projections of primary afferents in the spinal cord. Development 2005;132:2047–56.
[23] Dominici C, Moreno-Bravo JA, Puiggros SR, Rappeneau Q, Rama N, Vieugue P, Bernet A, Mehlen P, Chédotal A. Floor-plate-derived netrin-1 is dispensable for commissural axon guidance. Nature 2017;545:350–4.
[24] Dong HW. The Allen reference atlas: a digital color brain atlas of the C57Bl/6J male mouse. PsycNET. John Wiley & Sons Inc.,2008.
[25] Dostrovsky JO, Craig AD. Cooling-specific spinothalamic neurons in the monkey. J Neurophysiol 1996;76:3656–65.
[26] Dutton RC, Carstens MI, Antognini JF, Carstens E. Long ascending propriospinal projections from lumbosacral to upper cervical spinal cord in the rat. Brain Res 2006;1119:76–85.
[27] Esposito MS, Botta P, Chaudun F, Fadok JP, Markovic M, Wolff SBE, Ramakrishnan C, Fenno L, Deisseroth K, Herry C, Arber S, Tovote P, Lüthi A. Midbrain circuits for defensive behaviour. Nature 2016;534: 206–12.
[28] Fazeli A, Dickinson SL, Hermiston ML, Tighe RV, Steen RG, Small CG, Stoeckli ET, Keino-Masu K, Masu M, Rayburn H, Simons J, Bronson RT, Gordon JI, Tessier-Lavigne M, Weinberg RA. Phenotype of mice lacking functional Deleted in colorectal cancer (Dcc) gene. Nature 1997;386:796–804.
[29] Feil K, Herbert H. Topographic organization ot spinal ana trigeminal somatosensory pathways to the rat parabrachial and Kölliker—fuse nuclei. J Comp Neurol 1995;353:506–28.
[30] Francis JT, Xu S, Chapin JK. Proprioceptive and cutaneous representations in the rat ventral posterolateral thalamus. J Neurophysiol 2008;99:2291–304.
[31] Friocourt F, Kozulin P, Belle M, Suárez R, Di-Poï N, Richards LJ, Giacobini P, Chédotal A. Shared and differential features of Robo3 expression pattern in amniotes. J Comp Neurol 2019;527:2009–29.
[32] Gatto G, Goulding M. Locomotion control: brainstem circuits satisfy the need for speed. Curr Biol 2018;28:R256–9.
[33] Gauriau C, Bernard JF. A comparative reappraisal of projections from the superficial laminae of the dorsal horn in the rat: the forebrain. J Comp Neurol 2004;468:24–56.
[34] Giesler GJ, Spiel HR, Willis WD. Organization of spinothalamic tract axons within the rat spinal cord. J Comp Neurol 1981;195:243–52.
[35] Gutierrez-Mecinas M, Polgár E, Bell AM, Herau M, Todd AJ. Substance P-expressing excitatory interneurons in the mouse superficial dorsal horn provide a propriospinal input to the lateral spinal nucleus. Brain Struct Funct 2018;223:2377–92.
[36] Han S, Soleiman MT, Soden ME, Zweifel LS, Palmiter RD. Elucidating an affective pain circuit that creates a threat memory. Cell 2015;162:363–74.
[37] Helms AW, Johnson JE. Progenitors of dorsal commissural interneurons are defined by MATH1 expression. Development 1998;125:919–28.

[38] Hippenmeyer S, Vrieseling E, Sigrist M, Portmann T, Laengle C, Ladle DR, Arber S. A developmental switch in the response of DRG neurons to ETS transcription factor signaling. PLoS Biol 2005;3:e159–13.
[39] Hua ZL, Jeon S, Caterina MJ, Nathans J. Frizzled3 is required for the development of multiple axon tracts in the mouse central nervous system. Proc Natl Acad Sci USA 2014;111:E3005–14.
[40] Hubel DH, Wiesel TN. Anatomical demonstration of columns in the monkey striate cortex. Nature 1969;221:747–50.
[41] Hylden JL, Anton F, Nahin RL. Spinal lamina I projection neurons in the rat: collateral innervation of parabrachial area and thalamus. Neuroscience 1989;28:27–37.
[42] Jaworski A, Tom I, Tong RK, Gildea HK, Koch AW, Gonzalez LC, Tessier-Lavigne M. Operational redundancy in axon guidance through the multifunctional receptor Robo3 and its ligand NELL2. Science 2015;350: 961–5.
[43] Kahlson MA, Colodner KJ. Glial Tau pathology in tauopathies: functional consequences:. J Exp Neurosci 2016;9s2:JEN.S25515.
[44] Katter JT, Burstein R, Giesler GJ. The cells of origin of the spinohypothalamic tract in cats. J Comp Neurol 1991;303:101–12.
[45] Kennedy TE, Serafini T, la Torre Cell de JR, la Torre de JR, Tessier-Lavigne M. Netrins are diffusible chemotropic factors for commissural axons in the embryonic spinal cord. Cell 1994;78:425–35.
[46] Kitamura T, Yamada J, Sato H, Yamashita K. Cells of origin of the spinoparabrachial fibers in the rat: a study with fast blue and WGA-HRP. J Comp Neurol 1993;328:449–61.
[47] Kohro Y, Sakaguchi E, Tashima R, Tozaki-Saitoh H, Okano H, Inoue K, Tsuda M. A new minimally-invasive method for microinjection into the mouse spinal dorsal horn. Sci Rep 2015;5:14306.
[48] Krimpenfort P, Song JY, Proost N, Zevenhoven J, Jonkers J, Berns A. Deleted in colorectal carcinoma suppresses metastasis in p53-deficient mammary tumours. Nature 2012;482:538–41.
[49] Lai HC, Seal RP, Johnson JE. Making sense out of spinal cord somatosensory development. Development 2016;143:3434–48.
[50] Madisen L, Zwingman TA, Sunkin SM, Oh SW, Zariwala HA, Gu H, Ng LL, Palmiter RD, Hawrylycz MJ, Jones AR, Lein ES, Zeng H. A robust and high-throughput Cre reporting and characterization system for the whole mouse brain. Nat Neurosci 2010;13:133–40.
[51] Mantyh PW. The ascending input to the midbrain periaqueductal gray of the primate. J Comp Neurol 1982;211:50–64.
[52] Marsh APL, Heron D, Edwards TJ, Quartier A, Galea C, Nava C, Rastetter A, Moutard ML, Anderson V, Bitoun P, Bunt J, Faudet A, Garel C, Gillies G, Gobius I, Guegan J, Heide S, Keren B, Lesne F, Lukic V, Mandelstam SA, McGillivray G, McIlroy A, Méneret A, Mignot C, Morcom LR, Odent S, Paolino A, Pope K, Riant F, Robinson GA, Spencer-Smith M, Srour M, Stephenson SEM, Tankard R, Trouillard O, Welniarz Q, Wood A, Brice A, Rouleau G, Attié-Bitach T, Delatycki MB, Mandel J-L, Amor DJ, Roze E, Piton A, Bahlo M, Billette de Villemeur T, Sherr EH, Leventer RJ, Richards LJ, Lockhart PJ, Depienne C. Mutations in DCC cause isolated agenesis of the corpus callosum with incomplete penetrance. Nat Genet 2017;49:511–14.
[53] Matsushita M, Hosoya Y. Cells of origin of the spinocerebellar tract in the rat, studied with the method of retrograde transport of horseradish peroxidase. Brain Res 1979;173:185–200.
[54] Matsushita M, Hosoya Y, Ikeda M. Anatomical organization of the spinocerebellar system in the cat, as studied by retrograde transport of horseradish peroxidase. J Comp Neurol 1979;184:81–106.
[55] Menetrey D, Binder D, Besson JM. The origin of the spinomesencephalic tract in the rat: an anatomical study using the retrograde transport of horseradish peroxidase. J Comp Neurol 1982; 206:193–207.
[56] Menetrey D, de Pommery J. Origins of spinal ascending pathways that reach central areas involved in visceroception and visceronociception in the rat. Eur J Neurosci 1991;3:249–59.
[57] Mountcastle VB. Modality and topographic properties of single neurons of cat's somatic sensory cortex. J Neurophysiol 1957;20:408–34.
[58] Newman HM, Stevens RT, Apkarian AV. Direct spinal projections to limbic and striatal areas: anterograde transport studies from the upper cervical spinal cord and the cervical enlargement in squirrel monkey and rat. J Comp Neurol 1996;365:640–58.
[59] Nishida K, Ito S. Developmental origin of long-range neurons in the superficial dorsal spinal cord. Eur J Neurosci 2017;46:2608–19.
[60] Nornes HO, Carry M. Neurogenesis in spinal cord of mouse: an autoradiographic analysis. Brain Res 1978;159:1–6.
[61] Peng J, Ferent J, Li Q, Liu M, Da Silva RV, Zeilhofer HU, Kania A, Zhang Y, Charron F. Loss of Dcc in the spinal cord is sufficient to cause a deficit in lateralized motor control and the switch to a hopping gait. Dev Dyn 2018; 247:620–9.
[62] Petitjean H, Bourojeni FB, Tsao D, Davidova A, Sotocinal SG, Mogil JS, Kania A, Sharif-Naeini R. Recruitment of spinoparabrachial neurons by dorsal horn calretinin neurons. Cell Rep 2019;28:1429–38.e4.
[63] Pourchet O, Morel MP, Welniarz Q, Sarrazin N, Marti F, Heck N, Galléa C, Doulazmi M, Puiggros SR, Moreno-Bravo JA, Vidailhet M, Trembleau A, Faure P, Chédotal A, Roze E, Dusart I. Loss of floor plate Netrin-1 impairs midline crossing of corticospinal axons and leads to mirror movements. 2020 bioRxiv;84. 02.20.958595.
[64] Rabe Bernhardt N, Memic F, Gezelius H, Thiebes AL, Vallstedt A, Kullander K. DCC mediated axon guidance of spinal interneurons is essential for normal locomotor central pattern generator function. Dev Biol 2012;366:279–89.
[65] Renier N, Dominici C, Erzurumlu RS, Kratochwil CF, Rijli FM, Gaspar P, Chédotal A. A mutant with bilateral whisker to barrel inputs unveils somatosensory mapping rules in the cerebral cortex. eLife 2017;6:700.
[66] Rexed B. A cytoarchitectonic atlas of the spinal cord in the cat. J Comp Neurol 1954;100:297–379.
[67] Reynolds DV. Surgery in the rat during electrical analgesia induced by focal brain stimulation. Science 1969;164:444–5.
[68] Rustioni A, Kaufman AB. Identification of cells of origin of non-primary afferents to the dorsal column nuclei of the cat. Exp Brain Res 1977;27:1–14.
[69] Sabatier C, Plump AS, Le Ma, Brose K, Tamada A, Murakami F, Lee EYHP, Tessier-Lavigne M. The divergent Robo family protein rig-1/robo3 is a negative regulator of slit responsiveness required for midline crossing by commissural axons. Cell 2004;117:157–69.
[70] Sagner A, Briscoe J. Establishing neuronal diversity in the spinal cord: a time and a place. Development 2019:146:dev182154.
[71] Sengul G, Puchalski RB, Watson C. Cytoarchitecture of the spinal cord of the postnatal (P4) mouse. Anatomical Rec 2012;295:837–45.
[72] Spike RC, Puskár Z, Andrew D, Todd AJ. A quantitative and morphological study of projection neurons in lamina I of the rat lumbar spinal cord. Eur J Neurosci 2003;18:2433–48.
[73] Srour M, Rivière JB, Pham JMT, Dubé MP, Girard S, Morin S, Dion PA, Asselin G, Rochefort D, Hince P, Diab S, Sharafaddinzadeh N, Chouinard S, Théoret H, Charron F, Rouleau GA. Mutations in DCC cause congenital mirror movements. Science 2010;328:592.
[74] Szabo NE, da Silva RV, Sotocinal SG, Zeilhofer HU, Mogil JS, Kania A. Hoxb8 intersection defines a role for Lmx1b in excitatory dorsal horn neuron development, spinofugal connectivity, and nociception. J Neurosci 2015;35:5233–46.
[75] Todd AJ. Neuronal circuitry for pain processing in the dorsal horn. Nat Rev Neurosci 2010;11:823–36.
[76] Tripodi M, Stepien AE, Arber S. Motor antagonism exposed by spatial segregation and timing of neurogenesis. Nature 2011;479:61–6.
[77] Tulloch AJ, Teo S, Carvajal BV, Tessier-Lavigne M, Jaworski A. Diverse spinal commissural neuron populations revealed by fate mapping and molecular profiling using a novel Robo3Cre mouse. J Comp Neurol 2019; 527:2948–72.
[78] Varadarajan SG, Kong JH, Phan KD, Kao TJ, Panaitof SC, Cardin J, Eltzschig H, Kania A, Novitch BG, Butler SJ. Netrin-1 produced by neural progenitors, not floor plate cells, is required for axon guidance in the spinal cord. Neuron 2017;94:790–9.e3.
[79] Wentworth LE. The development of the cervical spinal cord of the mouse embryo. II. A Golgi analysis of sensory, commissural, and association cell differentiation. J Comp Neurol 1984;222:96–115.
[80] Willis WD, Trevino DL, Coulter JD, Maunz RA. Responses of primate spinothalamic tract neurons to natural stimulation of hindlimb. J Neurophysiol 1974;37:358–72.
[81] Witschi R, Johansson T, Morscher G, Scheurer L, Deschamps J, Zeilhofer HU. Hoxb8-Cre mice: a tool for brain-sparing conditional gene deletion. Genesis 2010;48:596–602.
[82] Xu K, Wu Z, Renier N, Antipenko A, Tzvetkova-Robev D, Xu Y, Minchenko M, Nardi-Dei V, Rajashankar KR, Himanen J, Tessier-Lavigne M, Nikolov DB. Structures of netrin-1 bound to two receptors provide insight into its axon guidance mechanism. Science 2014;344:1275–9.
[83] Zhang Y, Narayan S, Geiman E, Lanuza GM, Velasquez T, Shanks B, Akay T, Dyck J, Pearson K, Gosgnach S, Fan CM, Goulding M. V3 spinal neurons establish a robust and balanced locomotor rhythm during walking. Neuron 2008;60:84–96.